Authalic Parameterization of General Surfaces Using Lie Advection

Guangyu Zou, Jiaxi Hu, Xianfeng Gu, and Jing Hua, *Member, IEEE*

Abstract—Parameterization of complex surfaces constitutes a major means of visualizing highly convoluted geometric structures as well as other properties associated with the surface. It also enables users with the ability to navigate, orient, and focus on regions of interest within a global view and overcome the occlusions to inner concavities. In this paper, we propose a novel area-preserving surface parameterization method which is rigorous in theory, moderate in computation, yet easily extendable to surfaces of non-disc and closed-boundary topologies. Starting from the distortion induced by an initial parameterization, an area restoring diffeomorphic flow is constructed as a Lie advection of differential 2-forms along the manifold, which yields equality of the area elements between the domain and the original surface at its final state. Existence and uniqueness of result are assured through an analytical derivation. Based upon a triangulated surface representation, we also present an efficient algorithm in line with *discrete differential modeling*. As an exemplar application, the utilization of this method for the effective visualization of brain cortical imaging modalities is presented. Compared with conformal methods, our method can reveal more subtle surface patterns in a quantitative manner. It, therefore, provides a competitive alternative to the existing parameterization techniques for better surface-based analysis in various scenarios.

Index Terms—Area-preserving surface parameterization, differential forms, Lie advection, surface visualization.

1 Introduction

Surface parameterization refers to the process of mapping a surface into a canonical domain, which permits many surface operations to be performed in the parametric domain with improved efficiency and feasibility. It is of utmost importance in a broad range of graphics and visualization applications, such as texture mapping [24], remeshing [11], 3D shape analysis [18] and surface visualization [14].

To date, most parameterization techniques fall into two categories, namely, functional methods [28, 30, 34] and conformal methods [13, 24, 14, 22]. Functional methods typically start with defining certain penalty functions, such that the minima are assumed at desired results. Parameterization is then achieved using optimization methods. Although these methods are fairly flexible in terms of customizability to the properties to be preserved, in most cases, this approach can be problematic as the flattening is non-deterministic, relying on a set of tuning parameters and halting criteria. In general, no quantities are exactly preserved by the methods of this type. In contrast to those methods, conformal methods, on the other hand, possess several unique advantages, e.g., exact angle preserving, guarantee of solution existence, efficient implementations, and a rich continuous theory in parallel. However, a significant issue of conformal parameterization is that, especially when dealing with extruding shapes, the areal elements can be severely compressed for the price of preserving angular structure. Although it is known that additional surface cuts, along with cone singularities, can be introduced to the surface to effectively reduce the distortion of final results [22, 5, 31], such practice is *ad hoc* and can give rise to complications when data needs be accessed across the cut paths [11].

Despite a substantial literature devoted to surface and mesh parameterization, its area-preserving aspect has not been adequately studied or applied in this field. In many applications, such as quantitative analyses and visualization of *in vivo* brain surfaces [37], it is highly desirable that the fattened map, namely the parametric domain, can preserve area elements of the original brain surface, so that many area-related patterns derived from a rich line of multimodal information, e.g., neuronal density, activation extent, thickness, etc., can be accurately represented in this analytical space. Even though the distortion induced by parameterization procedures is notoriously undesired, it is well known that, in general, a surface cannot be flattened without any kinds of distortion in the presence of Gaussian curvature. For instance, conformal mapping can preserve local surface geometry by preserving angles no matter what conformal parameterization is chosen, however, the area stretching increases exponentially at the tip of protruding shapes.

In [7], Desbrun et al. showed that, based on a few desirable properties such as rotation and translation invariance, the only admissible parameterizations form a two-dimensional space spanned by the well-studied conformal parameterization and an area-preserving counterpart, namely, the authalic parameterization. They also explicitly stated that their formulation of *discrete authalic parameterization* was only a local minimum of a quadratic energy without known definition in differential geometry. Along this direction, there is no any existing technique which is rigorously area-preserving and meanwhile can be generalized to arbitrary surfaces. Prior area-preserving parameterizations typically strive for the local minima of certain objective functionals, which lack provable guarantee of area preservation.

In contrast, this paper presents a practical method to compute a group of global rigorous area-preserving parameterizations, which is mathematically rigorous and allows for an efficient implementation. Our method formulates the process of area restoration from an initial parameterization of arbitrary 2-manifolds using *Lie advection*, a frequently appearing concept in classical mechanics. To our best knowledge, this is the first work that employs Lie advection as a tool to manipulate area changes in the context of surface parameterization, which accommodates a wide range of boundary condition options. Besides a general framework, this work also features an efficient, yet accurate discretization scheme that is motivated by preserving the original geometric and algebraic structures of the continuous model in the limit, hence rendering better numerical fidelity and algorithmic scalability.

A similar idea was mathematically sketched in [3] and backed by a general result from [27] that guarantees the existence of an area-preserving diffeomorphism between two surfaces with the same total surface area. However, the discussion was restricted to a spherical domain. In this case, our mathematical derivation arrives at the same solution as [3]. Based on the Monge-Kantorovich theory of *optimal mass transport*, Haker et al. [15] developed an image registration and warping technique. Lying at the core is a decomposition of the deformation into a divergence-free vector field plus a curl-free one, called the *polar factorization*. A mass (e.g., area/volume) preserving mapping was explicitly sought in $\mathbf{R}^n$ by a gradient descent method to the Monge-Kantorovich functional. Their method has been used for area-

- *Guangyu Zou, Jiaxi Hu and Jing Hua are with Wayne State University, E-mail: {gyzou|jiaxihu|jinghua}@cs.wayne.edu.*
- *Xianfeng Gu is with State University of New York at Stony Brook, E-mail: gu@cs.sunysb.edu.*
- *Correspondence to Jing Hua.*

Manuscript received 31 March 2011; accepted 1 August 2011; posted online 23 October 2011; mailed on 14 October 2011.
For information on obtaining reprints of this article, please send email to: tvcg@computer.org.

preserving corrections on top of conformally flattened vessel surfaces in $\mathbf{R}^2$, implemented on a regular Cartesian grid [35]. Recently, the technique of optimal mass transport has also been applied to texture mapping of closed genus zero surfaces [8]. However, it is not clear how these methods can be extended to a general manifold. As a matter of fact, our analytical derivation as well as the implementation presented in this paper admits exact control of the finite areal dilation and shrinkage for the surface over the entire domain. Authalic parameterization is only a special case within a more versatile framework. Furthermore, our method can be readily generalized to compute the authalic mapping between two general manifolds equipped with nontrivial metrics, as the foundation of the system is formulated in *Discrete Exterior Calculus (DEC)*.

In summary, our proposed parameterization method has a number of prominent features, enumerated as follows:

- **Area-preserving supported by a rigorous continuous theory**. By introducing Lie advection to surface parameterization, the evolution of area elements can be precisely quantified by the Lie derivative. Computing an area-preserving parameterization is therefore equivalent to deriving a time-dependent vector field that corrects area distortions, i.e., dilation/shrinkage induced by an initial parameterization, through a diffeomorphic flow.

- **General to non-flat geometry of surfaces**. Our formulation is systematically based on the exterior calculus of differential forms. Thus, differential and integral equations can be conveniently expressed on smooth and curved spaces in a consistent manner. As our method is deeply-rooted to the intrinsic geometry of 2-manifolds, performing this procedure on non-flat domains, e.g., a unit sphere, is straightforward.

- **Extendable to surfaces of non-disc and closed-boundary topologies**, with and without surface cuts involved. This merit is largely inherited from the state-of-the-art conformal parameterization techniques [13, 22]. Given the initial parameterization, the subsequent evolution of the area elements essentially comprises an automorphism over the domain. The topological structure of the given parameterization remains intact.

- **Computationally affordable**. In general, the cost depends on the size of the mesh times the number of discretized steps needed for the desired accuracy. A satisfactory authalic parameterization can be usually obtained through solving a limited number of sparse, linear systems.

The remainder of the paper is organized as follows: Section 2 reviews the related work. The analytical foundation of our method is presented in Section 3. After that, we proceed to the technical details on the discrete algorithm in Section 4. The performance assessment as well as a demonstrative application to the surface-based multimodality analytics of brain imaging data is given in Section 5. Finally, in Section 6, we summarize our work and conclude with a discussion about the limitation, possible improvements as well as a few potential future directions of this method.

2 Related Work

Reducing area distortion of surface/mesh parametrization has been of major interest in the main geometry processing field. To prevent severe geometric stretches, on the one hand, the original model is typically decomposed into a set of charts homeomorphic to a disc in such a way that the interior Gaussian curvature is close to zero [24, 29, 30, 34], while on the other hand, various uniformity metrics have been applied to surface parameterizations to encourage even distribution of intrinsic distortions [28, 30, 21, 34]. Based on the singular values of the Jacobian matrix, Sander et al. [28] optimized the parametric location of each vertex within its 1-ring neighborhood to reduce local stretches. Sorkine et al.'s bounded-distortion paramterization [30] made heavy use of mesh cuts to keep distortions below some preset threshold. Zhang et al. [34] identified an anisotropic stretch term from a 2×2 tensor metric closely related to the one derived in [28] and applied it to guide the vertex optimization. Even though their distortion metric contains an area-preserving energy term, they did not mention whether an absolute area-preserving patch parameterization can be practically achieved. Desbrun et al. [7] also emphasized the importance of minimizing area distortion for the intrinsic parameterization of triangle meshes. In their work, an intuitive area-preserving functional was devised. Since the functional tried to preserve the area structure of the original 1-ring, the optimal parameterization derived was termed "Discrete Authalic Parameterization (DAP)". Due to the fact that the parameterization is only a critical point to the functional, it cannot exactly preserve areas across the mesh. Jin et al. [21] proposed to search for the optimal global conformal parameterization in the space of Möbius transformations. As conformality is invariant through Möbius transformations, the resulting parameterization is still conformal, which cannot completely eliminate area distortions. Based on the fact that surface parameterization is closely related to the topological constraints, delicate topological modifications can sometimes improve the uniformity of the parameterization. Towards this end, Gu and Yau punctured small holes at the tip of long appendages in [13]; Cone singularities were introduced with non-vanishing Gaussian curvature in [22, 5]; Surface cuts were repeatedly augmented according to the geometric stretches generated through the course of tentative parameterizations in [11]. Although such schemes provide excellent remedies to some applications, they are generally not acceptable to the rest. In terms of area preservation, these methods can be considered as heuristic approaches. Rigorous authalic parameterization is in general not achievable along this direction.

The analytical derivation of our method is consistently based on the differential forms on the manifold. Exterior calculus of differential forms has become a powerful tool in geometry processing for its clear revelation of the underlying geometric structures along with a well shaped mathematical foundation. In fact, most differential equation systems can be concisely formulated in the notion of differential forms. Holomorphic 1-forms were used for global conformal parameterization of nonzero genus surfaces in [13]. As this method is conformal, it potentially creates large area distortion, even after optimization [21]. The theoretical background concerned with several celebrated topological and geometric theorems, e.g., the Poincaré-Hopf index theorem and the Tutte's spring embedding theorem, was generalized in [10], based on the formalism of discrete 1-forms. Tong et al. [32] utilized harmonic 1-forms for surface quadrangulation and extended the discrete Laplacian operator to allow for a set of flexible meshing controls. Fisher et al. [9] demonstrated an interactive tangent vector field design system over arbitrary surface meshes, based on discrete 1-forms and the corresponding Laplacian operator. Recently, He et al. [16] applied harmonic 1-forms to skeleton extraction of 3D models. Because of its intrinsic nature, the system was demonstrated to be robust and can be generalized to different surface representations. While these works made extensive use of 0-forms and 1-forms, the computational primitive of our framework is 2-forms, which can be regarded as infinitesimal area elements on the manifold. Our application of differential forms is to quantify infinitesimal area changes of surfaces via a diffeomorphic flow formulated as a Lie advection.

3 Mathematical Theory

This section presents the analytical basis that leads to a family of rigorous authalic surface parameterizations. We refer interested readers to the appendix for the related concepts on diffeomorphism and differential forms.

Starting with an initial parameterization between a surface and its targeting domain, which requires to be a diffeomorphism (most modern parameterization methods [12, 24, 31] meet this requirement), we can homotopically deform it to an area-preserving one. Suppose M and Ω are the surface and desired domain to be parameterized upon, respectively. M and Ω are two differentiable 2-manifolds associated by a diffeomorphism $f : M \to \Omega$. The infinitesimal area elements of a surface can be mathematically depicted as differential 2-forms. Let ω_i, $i = M, \Omega$ be the area form of M and Ω, respectively. The pullback of

ω_Ω under f is a differential 2-form on M, denoted as $f^*(\omega_\Omega)$. We assume that M and Ω have the same area integral after a proper scaling, that is,

$$\int_M \omega_M = \int_\Omega \omega_\Omega. \tag{1}$$

Computing an area-preserving map $\mu : M \to \Omega$ now is equivalent to finding a diffeomorphism $\varphi : M \to M$, such that $\varphi^*(\omega_M) = f^*(\omega_\Omega)$. Consequently, μ is given by $f \circ \varphi^{-1}$.

To accomplish this, we first linearly interpolate a 2-form over time:

$$\omega_t = (1-t)\omega_M + t f^*(\omega_\Omega), \quad t \in [0,1]. \tag{2}$$

Note that $\omega_0 = \omega_M$ and $\omega_1 = f^*(\omega_\Omega)$. In the following, we will design a one parameter family of diffeomorphisms, such that the corresponding flow deforms the area element in the same fashion as ω_t. More specifically, consider a smooth surface M with a smooth vector field V on it. Given any point $p \in M$, there exists a unique integral curve $\gamma(t)$ of V passing through it, such that

$$\begin{cases} \frac{d\gamma_p(t)}{dt} = V(\gamma_p(t)), \\ \gamma_p(0) = p. \end{cases} \tag{3}$$

An one-parameter family of diffeomorphisms (which are also automorphisms) ϕ_t, parametrized by $t \in [0,1]$, can be defined on M as

$$\phi_t(p) = \gamma_p(t). \tag{4}$$

Here we need $\phi_t^*(\omega_0) = \omega_t$. Computing the time derivative at $t = 0$ on both sides, we get

$$\frac{d\phi_t^*\omega}{dt}\Big|_{t=0} = f^*(\omega_\Omega) - \omega_M, \tag{5}$$

which, by definition, is the *Lie derivative* of ω_t with respect to V. Hence, the central equation to solve is

$$\mathscr{L}_{V(t)}\omega_t = f^*(\omega_\Omega) - \omega_M, \tag{6}$$

where $\mathscr{L}_{V(t)}$ denotes the Lie derivative with respect to $V(t)$. By using Cartan's formula $\mathscr{L}_V = d(i_V) + i_V d$, where i_V denotes the interior product with respect to $V(t)$ and d the exterior derivative, we have

$$d(i_V\omega_t) + i_V d\omega_t = f^*(\omega_\Omega) - \omega_M. \tag{7}$$

Because ω_t is a 2-form on M, $d\omega_t = 0$. We therefore have

$$d(i_V\omega_t) = f^*(\omega_\Omega) - \omega_M. \tag{8}$$

Suppose h_M and h_Ω are two scaling factors (0-forms), such that $\omega_M = h_M du \wedge dv$ and $f^*(\omega_\Omega) = h_\Omega du \wedge dv$. Eq. 8 can be solved as

$$V(t) = \frac{1}{(1-t)h_M + t h_\Omega}\nabla g, \tag{9}$$

where

$$\Delta g = h_\Omega - h_M, \tag{10}$$

and Δ denotes the Laplacian-Beltrami differential operator. Note that, the above derivation only holds at $t = 0$. As system evolves over time, $V(t)$ varies in both magnitude and direction. Thus $V(t)$ needs to be solved at each time. Since g is essentially a harmonic scalar field on M (see Eq. (10)), the corresponding gradient vector field ∇g is guaranteed to be sufficiently smooth for integration and free of extraneous critical points. Time integration of $V(t)$ therefore yields a diffeomorphism. Note that pre-assignment of h_M essentially provides a straightforward mechanism to control infinitesimal area variation from the surface to the parameter domain. For an area-preserving mapping, $h_M = 1$. The following discussion sticks to this case. Finally, the proposed authalic parameterization is given by $f \circ \phi_{t=1}^{-1} : M \to \Omega$.

4 Algorithm

Now we discuss the discretization and algorithm corresponding to the theoretical result presented above. Most major mathematical concepts have existing conventional discrete forms [25], thus yielding a consistent computational framework which can be readily carried out in practice. More sophisticated discretization schemes can be interchangeably employed within the framework for the enhanced numerical approximation, which could be critical in certain extreme circumstances [4].

We approximate a surface by a triangular mesh $\Sigma = (V, E, F)$, where $V = \{v_i\}$ denotes the set of vertices, $E = \{e_{ij}\}$ the edge set, and $F = \{f_{ijk}\}$ the face set with $1 \le i, j, k \le n = |V|$. The position of vertex v_i is denoted by $\mathbf{v}_i \in \mathbf{R}^3$ and the edge vector corresponding to e_{ij}, which connects v_i to v_j, is $\mathbf{e}_{ij} = \mathbf{v}_j - \mathbf{v}_i$. The 1-ring neighbors of v_i are denoted as $N_1(i)$. All triangular faces assume counterclockwise orientation. Our algorithm is directly developed upon the structure of the original mesh.

For each vertex, the associated surface patch is chosen to be the barycentric finite volume, whose piecewise linear boundary connects the midpoints of the incident edges to the barycenters of adjacent triangles. Such finite volume configuration tiles the surface perfectly without overlap, i.e., each point on the surface is covered once and only once, and is insensitive to obtuse triangulations. Its value can be simply computed as

$$A_i = \frac{1}{6}\sum_{f_{ijk} \in N_1(i)} |\mathbf{e}_{ij} \times \mathbf{e}_{ik}|. \tag{11}$$

Geometric properties are averaged within the patch and retained at the center vertex. Our algorithm runs in two successive stages, which are illustrated in Fig. 1 using the brain hemisphere surface model. In the following, we describe each essential step of the algorithm in the order it occurs in the pipeline.

4.1 Initial Parameterization

In practice, we have chosen to use conformal parameterization to initialize our system, mainly for its robustness and abundant theoretical support. We first assume the target flat domain is a unit square, as is commonly used to parameterize topological disks. Later, we will show how this framework can be extended to accommodate more flexible boundary conditions. The square boundary condition is set up as follows: first, the boundary is isometrically mapped to that of the unit square D; next, a discrete conformal map of the interior is computed in the least squares fashion.

By selecting an arbitrary boundary vertex and assigning a corner of D to it, the initial boundary map can be sequentially laid out along ∂D, with consistent edge orientation relative to the original surface model. To avoid length distortion, we allocate for each edge an amount of the boundary proportional to its original length. Triangle degeneracies may incur when all the three vertices are on the boundary and mapped to one of the four sides of the square. Whenever such a triangle arises, we split its non-boundary edge(s) by inserting a new vertex at the midpoint. Moreover, when an edge spans one of the four corners of D, the edge is broken by introducing a vertex at the domain corner, thus splitting its incident triangle into two.

Having the boundary pinned down, the interior mapping can be solved via a linear system very efficiently, as detailed in [24]. The non-uniform local area stretching induced by the initial parameterization can be characterized by the finite model/parameter area ratio associated with each vertex v_i, denoted as λ_i. If the parameterization is conformal, λ is called the discrete *conformal factor*. Fig. 1(a) and 1(b) show the lateral and mesial views of a cortical hemisphere, respectively. The initial (conformal) parameterization is illustrated in Fig. 1(c), the area distortion of which is color encoded in Fig. 1(d). Some lateral cortical patterns suffer from the intensive geometric stretch which seriously impairs the inspection of these regions. Note that, the subsequent computation of authalic parameterization is deterministic to the initial parameterization provided. It is interesting to see how the

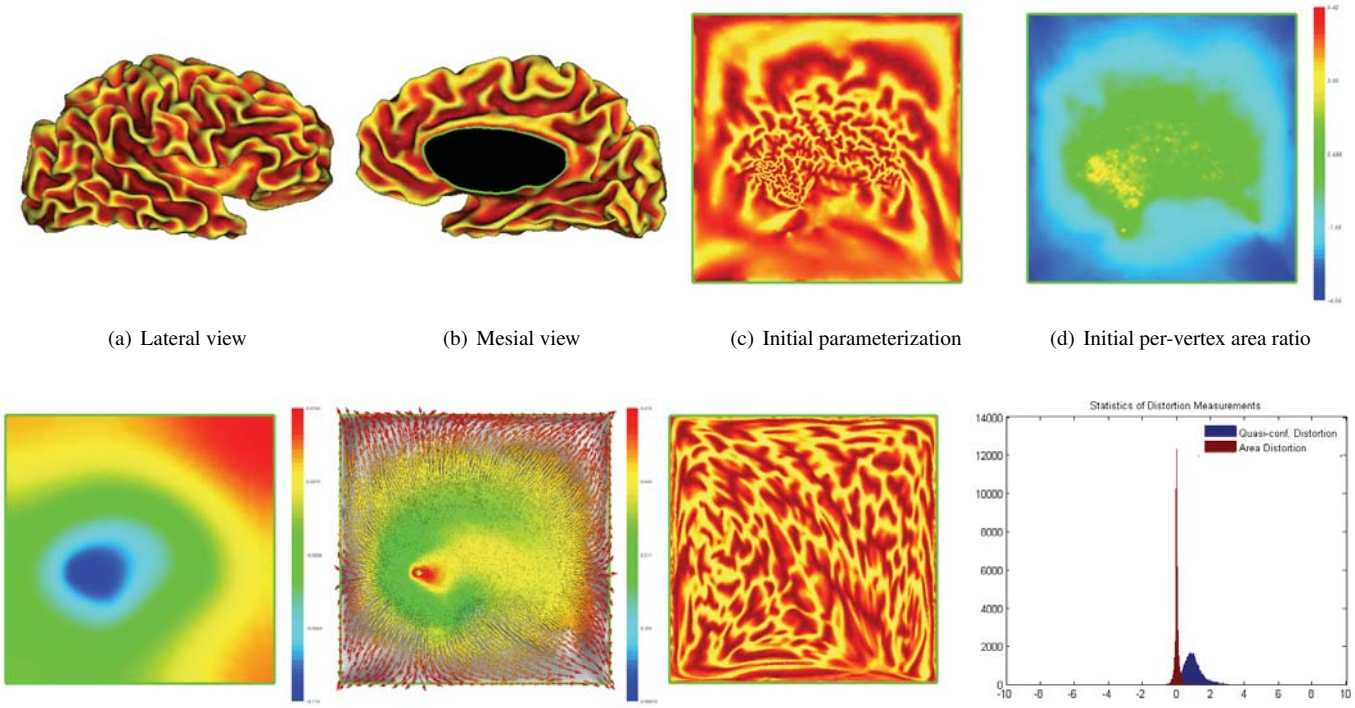

(a) Lateral view (b) Mesial view (c) Initial parameterization (d) Initial per-vertex area ratio

(e) Harmonic scalar field $g(t=0)$ (f) Gradient vector field $\nabla g(t=0)$ (g) Authalic parameterization $(t=1)$ (h) Area/angle distortion

Fig. 1. Algorithm pipeline. (a) and (b) give the lateral and the mesial views of a cortical hemisphere, respectively, which is provided for an authalic parameterization. We first compute an initial parameterization (c) of the surface on the targeted domain, e.g., using least square conformal map [24]; (d) shows the per-vertex model/parameter area ratio induced by (c). Based on the parameterization result generated, a harmonic scalar field is constructed on the domain, as shown in (e). Its gradient vector field is subsequently computed, as shown in (f). Finally, a dynamic diffeomorphic flow following the vector field direction is integrated over the time span of $[0,1]$ on the domain, which gives rise to the proposed authalic parameterization as shown in (g). (h) shows the statistics of the result in terms of area/angle distortion.

selection of initial parameterizations affects the numerical behaviors of the present computational pipeline. On the other hand, since our method can be performed upon any initial mapping, a wide range of surface parameterization methods are possible for the initial step in order to achieve particular functionalities relevant to the applications. An extensive comparative study in this regard is beyond the scope of this paper and will be conducted in the future.

4.2 Solving $\Delta g = h_\Omega - h_M$

For the purpose of area-preserving parameterization, h_M is always 1, whereas h_Ω is the per-vertex model/parameter area ratio at play. In accordance with Eq. (1), h_Ω is subject to a further normalization, such that the integral of h_Ω is equal to the total area of the domain.

Given a function f on the surface, its discrete version is a vector $\vec{g}$, defined on the vertex set V. To solve Eq. (10) on a triangular mesh, the discrete Laplace-Beltrami operator is linearly approximated at each vertex. Therefore, Δg is estimated at v_i as

$$\Delta g(v_i) = \frac{1}{A_i} \sum_{j \in N_1(i)} \frac{\cot \alpha_{ij} + \cot \beta_{ij}}{2} [g(v_j) - g(v_i)], \qquad (12)$$

where α_{ij} and β_{ij} are the two angles opposite to the edge e_{ij}, respectively. When considering all vertices of a mesh, Eq. (12) can be written as a linear system:

$$Lx = b, \qquad (13)$$

where $x = \vec{g}$ and $b = \vec{h}_\Omega - \vec{h}_M$. The involved matrix L represents the discrete Laplace-Beltrami operator, with its entries provided as follows:

$$L_{ij} = \begin{cases} \sum_{k \in N_1(i)} \frac{\cot \alpha_{ik} + \cot \beta_{ik}}{2A_i} & \text{if } i = j, \\ -\frac{\cot \alpha_{ij} + \cot \beta_{ij}}{2A_i} & \text{if } e_{ij} \in E, \\ 0 & \text{otherwise.} \end{cases} \qquad (14)$$

The matrix L is sparse. For this reason, Eq. (13) can be solved efficiently in linear time, e.g., using the preconditioned bi-conjugate gradient method. In practice, we have observed that solving the normal equations $L^T L x = L^T b$ yields more robust numerical behavior than directly solving Eq. (13). Fig. 1(e) shows the solved function g.

4.3 Computing ∇g

After the g is obtained, we can proceed to compute the corresponding gradient vector field on the triangulated domain. We consider a face f_{ijk} with its three corners lying at $\mathbf{v}_i$, $\mathbf{v}_j$, $\mathbf{v}_k$ in $\mathbf{R}^3$. Also, let $\mathbf{n}$ be a unit normal vector perpendicular to the plane spanned by f_{ijk}. Assuming linear interpolation within each triangle, the gradient vector can be easily computed by solving a 3×3 linear system:

$$\begin{bmatrix} \mathbf{v}_j - \mathbf{v}_i \\ \mathbf{v}_k - \mathbf{v}_j \\ \mathbf{n} \end{bmatrix} \nabla g = \begin{bmatrix} g_j - g_i \\ g_k - g_j \\ 0 \end{bmatrix}, \qquad (15)$$

for which an analytic solution exists. To obtain a unique vector at each vertex, ∇g at vertex v_i is defined as

$$\nabla g_i = \frac{1}{\sum_{f_{ijk} \in N_1(i)} \alpha^i_{jk}} \sum_{f_{ijk} \in N_1(i)} \alpha^i_{jk} \nabla g(f_{ijk}), \qquad (16)$$

that is, an average of the gradients of the adjacent faces, weighted by the incident angle α^i_{jk} of each face f_{ijk} at v_i. The resulting vector field

is shown in Fig. 1(f).

4.4 Time Integration of $V(t)$

Recall that the Lie derivative is defined as the instantaneous change of forms evaluated at $\phi_t(x)$, which is a dynamic definition (See Eq. (5)). Besides time t, $V(t)$ also depends on ∇g, which is in turn determined by the current vertex positions. For this reason, $V(t)$ needs to be updated at each step. Standard pathline computation is thus not applicable for the integration of $V(t)$. Instead, it is worth noticing that Eq. (9) can be analytically integrated as

$$\int_0^1 V(t)dt = \frac{\ln h_\Omega - \ln h_M}{h_\Omega - h_M}\nabla g. \tag{17}$$

In particular, when $h_M = 1$, we have

$$\lim_{h_\Omega \to 1} \frac{\ln h_\Omega - \ln h_M}{h_\Omega - h_M} = 1, \tag{18}$$

which means that, when h_Ω is sufficiently close to 1, the displacement vector field can be properly approximated by ∇g. Our scheme is therefore motivated by keeping the analytical portion of the computation as far as possible. Specifically, we divide the area-correcting process into K sequential steps. At each step, the area element is only modified by an small amount δh towards the target setting in such a way that the overall area adjustment is equal to $K\delta h$. For each area increment of δh, we let $h_\Omega = 1+\delta h$ and $h_M = 1$ as the input of the analytical integration (Eq. (17)), and the result gives the corresponding displacement with a change of δh in the area element as expected. To prevent the accumulation of numerical errors, in practice, we divide the remaining area excess into $K-k+1$ equal allotments at step k and compute h_Ω based on the current factual progress as

$$h_\Omega = 1 + \frac{\lambda_k - 1}{K-k+1}, \quad k = 1,\ldots,K, \tag{19}$$

where λ_k is given by the current per-vertex surface/domain area ratio at the beginning of step k. Let $V(v_i,k)$ denote the velocity field defined on the vertex set V of mesh Σ, at step k and $\phi(v_i,k)$ the induced mapping. By the one-parameter group structure of diffeomorphisms, $\phi(v_i,k)$ is simply the sum of all induced displacements of v_i plus the identity, written as

$$\phi(v_i,k) = \phi(v_i,0) + \sum_{i=1}^{k} \nabla g_i, \tag{20}$$

where $\phi(v_i,0)$ denotes the initial parameterization of the original mesh, and ∇g_i the gradient of function g solved at step i. Note that $\phi(V,K)$ gives the final discrete authalic map of mesh Σ at the end of the flow. The number of discrete steps is currently determined on a test-and-refine basis. In general, a larger number of iteration steps result in more accurate approximations. Empirically, discretizing this procedure into 50 steps can give satisfactory results for most mesh models. As our method essentially differs from an optimization framework, computation will not terminate until all the pre-determined steps have been completed. At the moment, boundary vertices are fixed. In the next section, we will show how this boundary condition can be relaxed. The final authalic parameterization of the cortical hemisphere is shown in Fig. 1(g). Fig. 1(h) presents the statistics of the area (dark red) and angle (blue) distortions; the employed metrics will be explained in Section 5.

The movement of vertices is in principle determined by the designated area changes. However, degenerate triangulation may undermine the discrete computation due to inaccurate approximation of the Laplace-Beltrami operator. Before each step begins, we optimize the underlying triangulation by performing combinatorial flips to all flippable edges opposite to the straight angles. Note that, the geometry of surfaces is realized by their $\mathbf{R}^3$ embedding. Throughout this procedure, the discrete sampling of the shape remains unchanged, but is merely interpolated by a different triangulation.

4.5 Boundary Conditions

Recent advances in conformal surface parameterization [22, 20, 5, 31] allow for a variety of rather flexible boundary conditions. Here, we demonstrate how our method can adapt to these boundary conditions, thus providing a seamlessly unified computational framework for area-preserving surface parameterization (flattening), in parallel with the state-of-the-art conformal mapping techniques.

4.5.1 Circular Boundaries

For non-closed surfaces, possibly with holes, we typically map them to certain canonical domains, such as disc or annulus, to facilitate various subsequent applications, such as 3D shape matching and registration [33, 36]. The centers and the radii of the boundary circles are either determined by certain heuristics or by the geometries of the original surface. It is therefore natural to restrict the boundary vertices to the domain boundaries, while letting them slide with the flow for an authalic parameterization. This motion is in fact induced by the covariant derivative of $V(t)$ in the tangential direction of domain boundary ∂D. As a conventional practice, whenever the vertex moves away from its inhabited space, it is subject to a projection along the radial direction to bring it back to the track. Fig. 2 demonstrates an example of applying the circular boundary condition to parameterizing surface models homeomorphic to a disk.

4.5.2 Sphere

Many surfaces in real life, such as the brain surface, are often modeled as a topological sphere, i.e., a closed surface of genus zero, thus is preferred to be parameterized on a unit sphere ($\mathbf{S}^2$) without any topological changes. Our method can easily adapt to this case as well. To achieve an initial parameterization of the surface onto the sphere, we compute its conformal mapping using the method described in [12]. The Lie advection flowing to the area preservation is then performed in the tangent spaces of such a spherical domain. To do so, we decompose the displacement vector field ∇g in each step into a normal component $\nabla^\perp g$ and a tangent component $\nabla^T g$. Let $\mathbf{n}$ denote the normal field of $\mathbf{S}^2$. For each vertex v_i, the normal component $\nabla^\perp g$ is computed as

$$\nabla^\perp g(v_i) = <\nabla g, \mathbf{n}>_{v_i} \mathbf{n}(v_i), \tag{21}$$

where $<\cdot,\cdot>$ is a scalar field, with its pointwise value defined as the inner product of two vectors in $\mathbf{R}^3$. Therefore, we also get its tangent component by

$$\nabla^T g = \nabla g - \nabla^\perp g. \tag{22}$$

We call $\nabla^T g$ the absolute displacement, since the domain is essentially evolved by the tangent component. In practice, whenever a vertex moves out of the unit sphere, it is pulled back by $v_i = v_i/|v_i|$. Fig. 3 demonstrates an example in this case, using the model Bimba with 39994 remeshed triangles.

4.5.3 Virtual Cuts

A recent advance in surface parameterization is represented by a string of conformal mapping techniques [22, 20, 5, 31] that allow global parameterizations of arbitrary surfaces via metric scaling within the class of conformal equivalence. For the final flat metric to be embedded over the Euclidean domain, a set of virtual cuts need to be introduced to the abstract manifold to open it to a topological disk. However, the parameterization remains global and continuous in that both sides along the cut can be perfectly adjoined under a rigid rotation and this property is independent of the placement of the cuts. The resulting parameterization is in fact a *fundamental domain* of the given surface, and the necessary cut paths can be determined by a homology basis. Now we demonstrate that an authalic counterpart sharing the same concept can be conveniently obtained in this framework.

Suppose the "virtual" cut made to the original surface is specified as a subset ρ of edges in Σ. For each non-boundary edge $e_{ij} \in \rho$, it is split into two mated boundary edges e_{ij}^+ and e_{ij}^-. A vertex v_i with n edges split in its 1-ring induces n equivalents $\{v_i^k\}$, $k = 0,\ldots,n-1$ in the resulting mesh. Given a pair of edge mates

(a) Model: Julius Caesar (b) Initial parameterization ($t=0$) (c) Authalic parameterization ($t=1$) (d) Area/angle distortion

Fig. 2. Authalic parameterization of a topological disk. (a) shows the Julius Caesar model containing 91780 triangles. This disk map (b) was generated using the discrete Ricci flow method [31]. The authalic parameterization is computed, as shown in (c), constrained by the circular boundary condition. The statistics of the result is shown in (d).

(a) Model: Bimba (b) Initial parameterization ($t=0$) (c) Authalic parameterization ($t=1$) (d) Area/angle distortion

Fig. 3. Authalic parameterization of a topological sphere. Similarly, (a) shows the Bimba model with 39994 triangles, which is a closed genus zero surface. Its spherical conformal parameterization is shown in (b). The corresponding authalic spherical parameterization is shown in (c). The statistics of the result is shown in (d).

(a) Model: Rocker Arm (b) Initial parameterization ($t=0$) (c) Authalic parameterization ($t=1$) (d) Area/angle distortion

Fig. 4. Authalic parameterization of a genus one surface. (a) shows the Rocker Arm model with 40088 triangles, with genus one topology. The cut paths are delineated in red. Its conformal parameterization is shown in (b). The corresponding authalic spherical parameterization is shown in (c). The statistics of the result is shown in (d).

$\{e_{ij}^{+} \in N_1(v_i^k), e_{ij}^{-} \in N_1(v_i^{k+1})\}$ where $N_1(v_i^k)$ and $N_1(v_i^{k+1})$ denote the respective 1-ring neighborhoods of v_i^k and v_i^{k+1} that share e_{ij} in the original mesh, a rigid motion $\mathscr{T}$ can be uniquely determined on the planar domain, such that $N_1(v_i^k)$ coincides with $\mathscr{T} \circ N_1(v_i^{k+1})$ exactly at e_{ij}^{+}. Since $\bigcup_{k=0}^{n-1} N_1(v_i^k) = N_1(v_i)$, the complete neighborhood structure of v_i can be reconstructed at v_i^k with corresponding edges perfectly aligned, pieced up in cyclic order by these partial 1-rings $\{N_1(v_i^k)\}, k = 0, \ldots, n-1$, dispersed among vertex equivalents. Whenever an operation is performed at v_i^k other than the vertices assigned with cone singularities, it is *de facto* treated as an ordinary vertex within the mesh. Fig. 4 demonstrates an example of parameterizing a genus one surface in the Euclidean 2D domain, in which the virtual cuts are incorporated after parameterization. Ideally, the shapes of the opposite boundaries should be identical by the nature of this treatment, which can be easily zippered back to the original model with continuity maintained across the cuts. Due to numerical errors induced in the computation of $\mathscr{T}$ and its subsequent application to the remote 1-ring pieces, those vertex equivalents fail to move consistently as time goes. As a result, the continuity of the original model across virtual cuts is

impaired after the diffemorphic flow. We are actively seeking better treatment for the vertices along the cut boundaries, such that the continuity can be preserved.

4.6 Summary of Algorithm

Our algorithm is summarized in Algorithm 1 as follows:

Algorithm 1 Authalic Surface Parameterization using Lie Advection

Input: The original model M; the target domain Ω; and the number of discretized steps n

1: Compute an initial parameterization $f : M \to \Omega$, e.g., using conformal mapping
2: **for** $i = 0$ **to** n **do**
3: Optimize triangulation (edge flipping)
4: Compute the areal ratio factor ($M/\Omega \to \lambda_i$)
5: Calculate h_Ω for each discretized step, such that $\lambda_{i+1} = \lambda_i + \delta h$
6: Solve the *Poisson equation* $\Delta g = \delta h$
7: Construct the gradient vector field ∇g
8: Apply the displacement field (approximated by ∇g) to the vertex set V
9: Boundary regularization (if boundary constraints exist)
10: **end for**

Output: An automorphism $\varphi : \Omega \to \Omega$, such that $f \circ \varphi^{-1}$ gives the final area-preserving parameterization

5 Experimental Results

Our system is implemented on 64-bit Windows 7 platform using C++. MATLAB computation engine is employed as a general purpose sparse linear solver and VTK/OpenGL for rendering and visualization. The experiments are conducted on an Intel T6600 2.20GHz laptop with 3GB RAM.

5.1 Numerics

Since finite volume has been used to compute the area ratio h_i, $i = M, \Omega$, we can reasonably expect good areal preservation in terms of areas associated with vertices. To verify that the area element is preserved globally regardless of the triangulation, we instead build up our distortion measures on their dual cells–triangular faces. To be specific, we examine both the area distortion and the quasi-conformal distortion per face over the mesh. The area distortion metric Υ and the quasi-conformal distortion metric Λ are computed respectively as follows:

$$\Upsilon = \ln(\gamma_{max} \cdot \gamma_{min}), \quad \Lambda = \ln \frac{\gamma_{max}}{\gamma_{min}}, \tag{23}$$

where $(\gamma_{max}, \gamma_{min})$ are the larger and smaller eigenvalues of the Jacobian of the affine transformation that maps the domain triangle to the surface, normalized in such a way that the total area of the surface equals that of the domain, as described in [28]. γ_{max} and γ_{min} represent the largest and smallest local stretches among all possible directions when mapping a non-zero vector from the domain to the surface. For a conformal parameterization, we need $\gamma_{max} = \gamma_{min}$ ($\Lambda = 0$), while $\gamma_{max} \cdot \gamma_{min} = 1$ ($\Upsilon = 0$) means area preservation. In both cases, a value of 0 indicates no distortion at all. A mapping is isometric, if and only if $\Upsilon = \Lambda = 0$. The advantages of using logarithmic values for the metrics include 1) the ideal (no distortion) is therefore unified to the axis origin (0); and 2) the bias between stretches along the two orthogonal eigen-directions is eliminated.

The statistics of the area and the quasi-conformal distortions are given for all the examples, respectively. The X axis denotes the values of distortion metrics Υ and Λ, while the reading of Y axis denotes the number of triangles that bear the corresponding distortion metrics. As shown by the dark red histograms, the distribution of Υ is highly concentrated about zero, meaning that the area of triangles are well preserved throughout all the experiments. For general surfaces with non-trivial Gaussian curvature, it is in general impossible for a mapping to be both area-preserving and angle-preserving, i.e., isometric, as theoretically confirmed by the classical results from Riemannian geometry. Hence, area preservation will inevitably induce angle distortion, which in fact is expectable after application of the aforementioned parameterization procedure. For this reason, the distribution of Λ spans from 0 to 3 without any obvious patterns. However, as visually demonstrated by these examples, the induced angle distortion is not significant. From the experiments, we also notice that the severe distortion is concentrated at the boundary and spread very little inwards. This is because, while constrained by each particular boundary condition, boundary vertices cannot freely moves as directed by the area restoring flow ($V(t)$). Thus, the area manipulation is not fully enforced on the boundary.

Table 1. Numerical Results of Examples Shown throughout This Paper

Fig.	$\|F\|$	Iter.	Time	Init. Map
1 (Brain Hemisphere)	48287	50	57s	[24]
2 (Julius Caesar)	91780	50	2m:14s	[31]
3 (Bimba)	39994	50	50s	[12]
4 (Rocker Arm)	40088	150	2m:49s	[31]
5 (Full Brain)	99738	200	8m:32s	[24]

Table 1 summarizes the numerical results of our experimental implementation, which is indexed by the figure number (column 1) and includes information about mesh sizes (column 2), the number of discretization steps (column 3), the computation times taken(column 4), and the methods used for the initial parameterization (column 5). The computation times only account for the procedure of authalic area correction based on the initial inputs. As we can see from Table 1, the computation times scale linearly in accordance with mesh sizes and the number of iterations.

5.2 Quantitative Surface-based Analytics

Although the presented method is applicable to general surfaces in principle, of particular interest to us are its applications to brain imaging modality visualization and analytics. Many neurological phenomena can be indicated by changes in the various brain imaging measurements. With a focus on the cerebral cortex, which plays a key role in many aspects of human intelligence and is profoundly associated with a variety of brain diseases and neurological disorders, we briefly introduce a visual analysis framework that is designed to integrate various complementing neuroimaging modalities from multiple sources, so that quantitative assessments from individual modalities can be formalized into a unified data structure to facilitate advanced data mining and visualization.

In this application, surface parameterization (flattening) constitutes a major means of visualizing highly convoluted anatomical surfaces, allowing clear examination of many pathologies once deeply buried within the folds [19]. Moreover, cross-subject analysis of brain cortical structures and functions needs, as a prerequisite step, the alignment of homologous regions. By parameterizing brain surfaces on a common domain, they are naturally correlated via homotopic parameter coordinates. Suppose M_1 and M_2 are two brain surfaces, and $\varphi_1 : M_1 \to \mathbf{R}^2$ and $\varphi_2 : M_2 \to \mathbf{R}^2$ are the parameterizations, respectively. Through the composition $\varphi_2^{-1} \circ \varphi_1 : M_1 \to M_2$, a one-to-one correspondence is defined between M_1 and M_2. To simplify the process, 3D surfaces can be represented as a shape vector image $\vec{g}(u,v)$ retained in a 2D domain [18], where the co-registered modalities are uniformly indexed by regular pixels. In this procedure, the brain surface is sliced open along the medial plane at the bottom, without passing any significant anatomical features. The entire brain surface is then mapped to a rectangle with the height/width ratio equal to 1:2. In almost all situations, the top and lateral portions of the brain surface, where the most meaningful anatomies and functional regions reside, are squeezed into a very small area of the domain after the conformal mapping (Fig. 5(c)). With the uniform sampling through the entire domain, shape vector images turn out not to have enough samples, at the

locations with severely squeezed distortion, to capture the geometric as well as neurological characteristics of the brain cortex. This issue is well addressed by employing our newly proposed approach. As shown in Fig. 5(d), now the surface sampling is much more evenly distributed. The shading effects are generated by using the original normals in order to visualize the correspondence between the brain surface and the rectangular domain.

Normal brain function is dependent on the interactions between specialized regions of the brain which process information with local and global neurological networks. To capture the statistics of abnormal brain activity, a sufficient number of sampling points should be grouped at certain resolution. Each unit forms a cortical element. Since the surface of the brain is uneven and varies across human subjects, the task of subdividing it into a set of equal geometric elements is nontrivial. Instead, we can easily define finite homotopic cortical elements in the parametric domain with simple isotropic grid, as shown in Fig. 5(c) and 5(d). Then, the elements can be reversely mapped back into the subject's native space, probing any modalities of interest. Note that, thanks to the area-preserving property of the proposed parameterization method, each element accounts for an identical amount of portion in the original brain surface. For the purpose of comparison, we also include a parametric domain generated by the conformal parameterization. Two homotopic cortical elements are highlighted in red and blue, respectively. Using conformal parameterization, the element highlighted in red will be assigned with excessive cortical area, while for the element highlighted in blue, little feature is covered. This drawback is greatly eliminated by using the authalic parameterization. As shown in Fig. 5(d), both elements can capture an equal patch on the brain surface. With these well-defined equiareal cortical elements, a variety of functional patterns can be readily quantified on a per element basis. In our experiment, the functional characteristics of brain cortical activation is captured by Positron Emission Tomography (PET), while the detailed structural information is obtained from Magnetic Resonance Imaging (MRI). In order to integrate PET and MRI data, a normal fusion approach is performed in the native space of each subject, as illustrated in Fig. 5(a). Typically, the PET tracer concentration is calculated by averaging its measurement along the inverse normal direction within $10mm$ from the cortical surface. The obtained value is then mapped to the brain surface (Fig. 5(b)). Once normative brain patterns for each element are derived from a group of control subjects, whether a particular cortical element derived from a patient falls into the abnormal can be subsequently determined according to the comparison against the normative reference. The PET deviation degree is the basis for the classification of functional abnormality of cortical elements. This framework allows consistent integration and quantitative analysis of multiple functional brain patterns. The inclusion of other imaging data such as gray matter thickness measured by MRI is conceivable. Since in reality the deviation degrees of different modalities rarely coincide, it is interesting and important to examine the degree of agreement among several modalities and its statistical significance. We will explore along this direction in the future work.

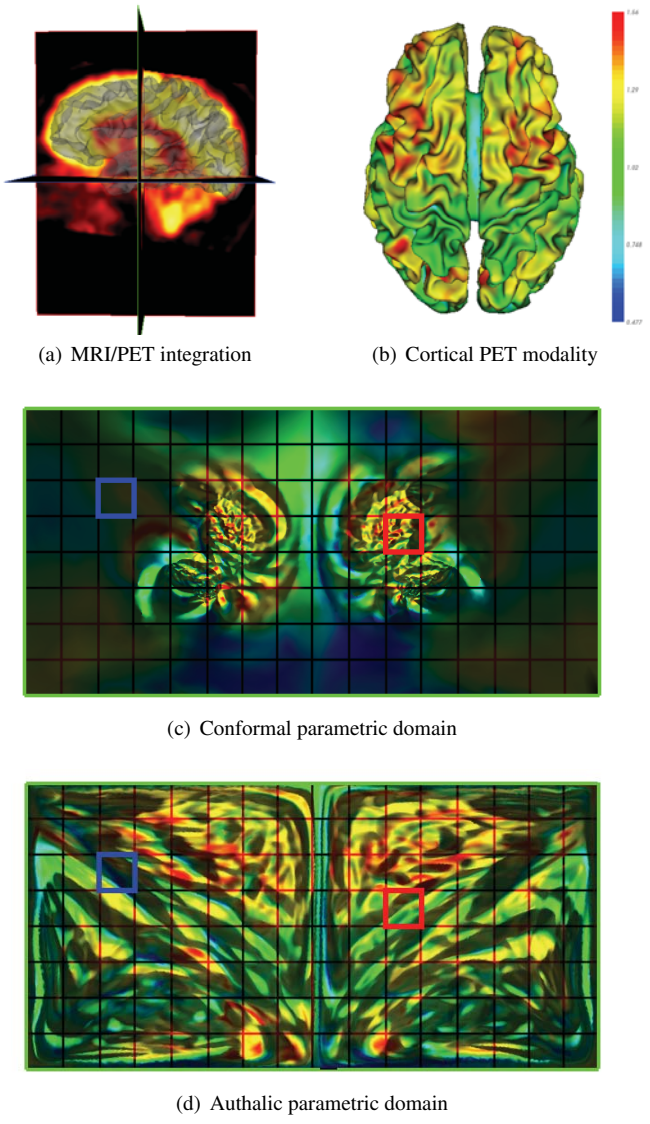

(a) MRI/PET integration (b) Cortical PET modality

(c) Conformal parametric domain

(d) Authalic parametric domain

Fig. 5. Application of quantitative surface-based analytics. (a) Integration of functional Positron Emission Tomography (PET) imaging data and the structural Magnetic Resonance Imaging (MRI) imaging data; (b) the brain surface mapped with the PET value. (c) the parametric domain generated using conformal parameterization; (d) the parametric domain generated using the proposed authalic parameterization.

6 Conclusion

In this paper, we have presented a surface parameterization methodology that is rigorously area-preserving in its continuous theory. Given an initial parameterization, an area-preserving one can be efficiently and uniquely obtained via the Lie advection of area forms along the domain. This approach can be easily extended to parameterize more general surfaces as long as the initial parameterization is provided. Our implementation strives to preserve the analytical ingredients of the computation as far as possible. As a result, our method only involves moderate computation and is stable in getting consistent results, as opposed to an optimization approach. We have also demonstrated the utility of our method by creating area-preserving maps of both cortical hemispheres and the entire cortex. As shown in the figures and the statistics throughout the experiments, the property of preserving area structure of the original surface may better facilitate present quantitative analysis frameworks for various neuroimaging data.

A known limitation of the cotangent formulation of Laplace-Beltrami operator is that it deals not well with degenerate meshes. Adaptive edge flipping and subdivision may alleviate this problem to some extent. Alternatively, more delicate and robust approximation schemes of Laplace-Beltrami operator, such as the one recently proposed in [4], could be used when presented with extremely skinny triangles.

We have observed that long protrusions can result in severe squeezing effects on a flat domain in areas approaching their bases. Because for general manifolds, no isometric mapping exists except for a few special cases, it is essentially a compromise at the expense of area preservation. However, a rigorous area-preserving parameterization technique is still of fundamental importance in both theoretical and practical senses, as it answers the open problem left in [7] by showing that, other than the conformal mapping, its authalic counterpart can be practically found in a mathematically rigorous manner.

Besides surface parameterization, another potential area that may benefit from this work is point-based graphics [2, 1]. When it deals with implicit surface and point set surface visualization, a major issue

is to redistribute sampling points within a surface to facilitate compact and flexible modeling of 3D objects. The underlying computational model is typically a dynamical particle system [26]. Based on some local potential energy profiles, the inter-particle forces determine the final density and location of sampling points [23]. It is not surprising that the involved computation is expensive. And similar to functional parameterization methods, it gives rise to the common pitfalls of optimization-based approaches. Our method provides a radically different mechanism to control point samples and distribute them according to the needs of applications, which is formulated in the language of differential forms on the manifold. Exact sample spacing control can be achieved via a prescription of area scaling factor. Unlike most classical methods, the computation is deterministic. The particle system generated using our method can provide a uniform sampling density over the surface from the parametric domain, but not isotropic in general.

We believe the computational performance and runtime for this approach can still be improved. A multiresolution mesh representation, e.g., [17], can be directly incorporated into our method, giving rise to a hierarchical, coarse-to-fine approach. Beside brain surface mapping, we also envision a broad range of applications of Lie advection in graphics, geometric modeling and visualization, such as geometry images [11], point-set surfaces [1], and glyph packing [23].

APPENDIX

A DIFFEOMORPHISM

Suppose M and N are two differentiable manifolds, a bijective map $f : M \to N$ is a diffeomorphism if and only if f and its inverse f^{-1} are both differentiable. All diffeomorphisms of M to itself are called the *diffeomorphism group* of M. Here we denote it as $Diff(M)$. A prominent advantage of diffeomorphisms, compared with other maps, is that the neighborhood structure is preserved, i.e., connected sets remain connected while disjoint ones remain disjoint, and the coordinates are transformed smoothly. For this reason, diffeomorphism has become a major non-rigid deformation model used for image registration and comparison. Suppose Ω is the domain that sustains the diffeomorphic transformation $\varphi : \Omega \to \Omega$. Computation of φ typically involves a smooth time-dependent vector field $v : \Omega \times [0,1] \to V$ where V is a Hilbert space of smooth, compactly supported vector fields on Ω, such that φ is estimated as the end point of the flow associated with $v(\Omega,t)$, $t \in [0,1]$. More specifically, the evolution of a curve ϕ^v in the space of diffeomorphisms $Diff(M)$ can be defined via a transport equation

$$\frac{d\phi_t^v(x)}{dt} = v_t(\phi_t^v(x)). \tag{24}$$

The function $\phi_t^v(x)$ bears the one-parameter (time) group structure, that is, $\phi_s^v(\phi_t^v(x)) = \phi_{s+t}^v(x)$ with $\phi_0^v(x) = x$ for all $s,t \in \mathbf{R}$. Integrating Eq. (24) over time t,

$$\varphi(x) = \phi_0^v(x) + \int_0^1 \phi_t^v(x)dt, \quad x \in \Omega, \tag{25}$$

gives a diffeomorphism $\varphi(x) = \phi_1^v(x)$ with $\phi_0^v(x) = Id$. In practice, $\varphi(x)$ can be efficiently computed in the Lagrangian frame. The diffeomorphic flow is observed by following the streamlines of running particles. Lagrangian-like schemes are known to be computationally stable and provide good tolerance to numerical-accuracy related errors for the choice of time step.

B DIFFERENTIAL FORMS

Differential forms are at the foundation of modern differential geometry, which consistently express integral and differential equations on smooth and curved spaces in a coordinate-independent way. Moreover, they often reflect underlying geometric structures and invariants in concise forms. Formally, let M be a smooth manifold. All tangential vectors at a point $p \in M$ form a vector space T_pM, namely the tangent space to M at p. A k-form ω^k is an anti-symmetric, covariant tensor field of rank-k over M, such that at each point $p \in M$, ω^k defines a multi-linear map

$$\omega^k : T_pM \times \cdots \times T_pM \to \mathbf{R}, \tag{26}$$

which changes signs for odd permutations of the components. Note that a sub-manifold of M naturally inherits a k-form from M by restricting the linear map to the domain that is the product of tangent spaces of the sub-manifold.

We consider surfaces as 2-manifolds embedded in $\mathbf{R}^3$. In such a case, non-zero forms only exist for dimensions ranging from 0 and 2, which can be intuitively conceived as a scalar field for 0-form, a tangent vector field for 1-form, and a bivector (induced by two coplanar vectors) field for 2-form. In turn, applying forms to vector fields amounts to

- 0-form: $\omega^0(v) \equiv \omega^0 v$;
- 1-form: $\omega^1(v) \equiv \omega^1 \cdot v$;
- 2-form: $\omega^2(u,v) \equiv \omega^2 \cdot (u \times v)$.

To facilitate formulation of how the authalic surface mapping is derived, we also introduce a set of essential operators that are used to manipulate differential forms:

- Exterior Derivative (d). It generalizes the notion of the differential of a function to forms. According to the rank k of the form ω^k, d corresponds to the gradient ∇, the curl $\nabla\times$, and the divergence $\nabla\cdot$, when $k = 0,1,2$, respectively.
- Hodge Star ($\star$). It maps a k-form to a complementary $(n-k)$-form. According to the dimension of the form, we define it as

$$\star f = f du \wedge dv,\ \star du = dv,\ \star dv = -du,\ \star f du \wedge dv = f.$$

- Wedge Product ($\wedge$). It constructs a higher degree form by $\omega^{i+j} = \omega^i \wedge \omega^j$, extending the notion of exterior product to forms. In $\mathbf{R}^3$, the wedge product of two 1-forms, α and β, can be identified via the standard cross product as $\alpha \wedge \beta \equiv \alpha \times \beta$.
- Interior Product (i_V). It is defined to be the contraction of a differential form with a vector field V. In our case, it can be computed as

$$i_V \omega^1 = \omega_1 \cdot V, \quad i_V \omega^2 = \omega_2 \times V.$$

- Lie Derivative ($\mathscr{L}_V$). When defined on differential forms, it extends the notion of directional derivative, which instead estimates the change of one form along the flow of the given vector field V. By *Cartan's homotopy identity*, $\mathscr{L}_V = d(i_V) + i_V d$.

Beware that our definition of operators is specific to surfaces. Care should be taken when extending them to other spaces. We also refer readers to [6] and references therein for a complete exposition of differential forms in the context of computational modeling.

The area element indeed is a 2-form on the surface, which acts on two tangent vectors $\mathbf{u},\mathbf{v} \in TS_p$ given a point p, and returns the area of the parallelogram spanned by them. Consider a diffeomorphism $f : M \to N$ with ω_N being the area element on N. The pullback of ω_N is a 2-form on M, denoted as $f^*(\omega_N)$, and defined as

$$f^*(\omega_N)(\mathbf{u},\mathbf{v}) = \omega_N(df(\mathbf{u}), df(\mathbf{v})). \tag{27}$$

ACKNOWLEDGMENTS

We would like to thank the reviewers for their valuable comments. This work is supported in part by the grants awarded to Jing Hua, including the National Science Foundation grants IIS-0915933, IIS-0937586, and IIS-0713315, as well as the National Institute of Health grants 1R01NS058802-01A2 and 2R01NS041922-05A1.

REFERENCES

[1] M. Alexa, J. Behr, D. Cohen-Or, S. Fleishman, D. Levin, and C. T. Silva. Computing and rendering point set surfaces. *IEEE Trans. on Vis. Comput. Graph.*, 9(1):3–15, 2003.

[2] N. Amenta and Y. J. Kil. Defining point-set surfaces. *ACM Trans. Graph.*, 23(3):264–270, 2004.

[3] S. Angenent, S. Haker, A. Tannenbaum, and R. Kikinis. On area preserving mappings of minimal distortion. In T. Djaferis and I. Schick, editors, *System Theory: Modeling, Analysis, and Control*. Kluwer, Holland, 1999.

[4] M. Belkin, J. Sun, and Y. Wang. Discrete laplace operator on meshed surfaces. In *Proceedings of the 24th symp. on computational geometry*, pages 278–287, 2008.

[5] M. Ben-Chen, C. Gotsman, and G. Bunin. Conformal flattening by curvature prescription and metric scaling. *Comput. Graph. Forum*, 27(2):449–458, 2008.

[6] M. Desbrun, E. Kanso, and Y. Tong. Discrete differential forms for computational modeling. In *SIGGRAPH '05: ACM SIGGRAPH 2005 Courses*, page 7, 2005.

[7] M. Desbrun, M. Meyer, and P. Alliez. Intrinsic parameterizations of surface meshes. *Comput. Graph. Forum*, 21:209–218, 2002.

[8] A. Dominitz and A. Tannenbaum. Texture mapping via optimal mass transport. *IEEE Trans. on Vis. Comput. Graph.*, 16(3):419–433, 2010.

[9] M. Fisher, P. Schröder, M. Desbrun, and H. Hoppe. Design of tangent vector fields. *ACM Trans. Graph.*, 26(3), 2007.

[10] S. J. Gortler, C. Gotsman, and D. Thurston. Discrete one-forms on meshes and applications to 3d mesh parameterization. *Comput. Aided Geom. Des.*, 23(2):83–112, 2006.

[11] X. Gu, S. J. Gortler, and H. Hoppe. Geometry images. *ACM Trans. Graph.*, 21(3):355–361, 2002.

[12] X. Gu, Y. Wang, T. F. Chan, P. M. Thompson, and S. tung Yau. Genus zero surface conformal mapping and its application to brain surface mapping. *IEEE Trans. Med. Imag.*, 23:949–958, 2003.

[13] X. Gu and S.-T. Yau. Global conformal surface parameterization. In *Proc. the 2003 Eurographics symp. on geometry processing*, pages 127–137, 2003.

[14] S. Haker, S. Angenent, A. Tannenbaum, R. Kikinis, G. Sapiro, and M. Halle. Conformal surface parameterization for texture mapping. *IEEE Trans. on Vis. Comput. Graph.*, 6(2):181–189, 2000.

[15] S. Haker, L. Zhu, A. Tannenbaum, and S. Angenent. Optimal mass transport for registration and warping. *Int. J. Comput. Vision*, 60(3):225–240, 2004.

[16] Y. He, X. Xiao, and H.-S. Seah. Harmonic 1-form based skeleton extraction from examples. *Graph. Models*, 71(2):49–62, 2009.

[17] H. Hoppe. Progressive meshes. In *Proceedings of SIGGRAPH '96*, pages 99–108, 1996.

[18] J. Hua, Z. Lai, M. Dong, X. Gu, and H. Qin. Geodesic distance-weighted shape vector image diffusion. *IEEE Trans. on Vis. Comput. Graph.*, 14(6):1643–1650, 2008.

[19] M. Hurdal, K. Kurtz, and D. Banks. Case study: Interacting with cortical flat maps of the human brain. In *Proceedings of VIS '01*, pages 469–472, 2001.

[20] M. Jin, J. Kim, F. Luo, and X. Gu. Discrete surface ricci flow. *IEEE Trans. on Vis. Comput. Graph.*, 14(5):1030–1043, 2008.

[21] M. Jin, Y. Wang, S.-T. Yau, and X. Gu. Optimal global conformal surface parameterization. In *Proceedings of VIS '04*, pages 267–274, 2004.

[22] L. Kharevych, B. Springborn, and P. Schröder. Discrete conformal mappings via circle patterns. *ACM Trans. Graph.*, 25(2):412–438, 2006.

[23] G. Kindlmann and C.-F. Westin. Diffusion tensor visualization with glyph packing. *IEEE Trans. on Vis. Comput. Graph.*, 12(5):1329–1335, 2006.

[24] B. Lévy, S. Petitjean, N. Ray, and J. Maillot. Least squares conformal maps for automatic texture atlas generation. *ACM Trans. Graph.*, 21(3):362–371, 2002.

[25] M. Meyer, M. Desbrun, P. Schröder, and A. H. Barr. Discrete differential-geometry operators for triangulated 2-manifolds. In *VisMath '02*, pages 35–57, 2002.

[26] M. D. Meyer, P. Georgel, and R. T. Whitaker. Robust particle systems for curvature dependent sampling of implicit surfaces. In *Proc. the Int'l Conf. on Shape Modeling and Applications (SMI)*, pages 124–133, 2005.

[27] J. Moser. On the volume elements on a manifold. *AMS Trans.*, 120(2):286–294, 1965.

[28] P. V. Sander, J. Snyder, S. J. Gortler, and H. Hoppe. Texture mapping progressive meshes. In *Proceedings of SIGGRAPH '01*, pages 409–416, 2001.

[29] P. V. Sander, Z. J. Wood, S. J. Gortler, J. Snyder, and H. Hoppe. Multi-chart geometry images. In *Proceedings of the 2003 Eurographics/ACM SIGGRAPH symp. on Geometry processing*, pages 146–155, 2003.

[30] O. Sorkine, D. Cohen-Or, R. Goldenthal, and D. Lischinski. Bounded-distortion piecewise mesh parameterization. In *Proceedings of VIS '02*, pages 355–362, 2002.

[31] B. Springborn, P. Schröder, and U. Pinkall. Conformal equivalence of triangle meshes. *ACM Trans. Graph.*, 27(3):77:1–77:11, 2008.

[32] Y. Tong, P. Alliez, D. Cohen-Steiner, and M. Desbrun. Designing quadrangulations with discrete harmonic forms. In *Proc. the fourth Eurographics symp. on Geometry processing*, pages 201–210, 2006.

[33] W. Zeng, D. Samaras, and X. D. Gu. Ricci flow for 3d shape analysis. *IEEE Trans. Pattern Anal. Mach. Intell.*, 32:662–677, 2009.

[34] E. Zhang, K. Mischaikow, and G. Turk. Feature-based surface parameterization and texture mapping. *ACM Trans. Graph.*, 24(1):1–27, 2005.

[35] L. Zhu, S. Haker, and A. Tannenbaum. Flattening maps for the visualization of multibranched vessels. *IEEE Trans. Med. Imaging*, 24(2):191–198, 2005.

[36] G. Zou, J. Hua, Z. Lai, X. Gu, and M. Dong. Intrinsic geometric scale space by shape diffusion. *IEEE Trans. on Vis. Comput. Graph.*, 15(6):1193–1200, 2009.

[37] G. Zou, J. Hua, and O. Muzik. Non-rigid surface registration using spherical thin-plate splines. In *Proceedings of the 10th International Conference on Medical Image Computing and Computer Assisted Intervention*, pages 367–374, 2007.